

ON THE CONTRIBUTION OF FLUORESCENCE TO LYMAN ALPHA HALOS  
AROUND STAR FORMING GALAXIESLLUÍS MAS-RIBAS<sup>1</sup> AND MARK DIJKSTRA

Institute of Theoretical Astrophysics, University of Oslo, P.O. Box 1029 Blindern, N-0315 Oslo, Norway

*Draft version April 5, 2024*

## ABSTRACT

We quantify the contribution of Ly $\alpha$  fluorescence to observed spatially extended Ly $\alpha$  halos around Ly $\alpha$  emitters (LAE) at redshift  $z = 3.1$ . The key physical quantities that describe the fluorescent signal include (i) the distribution of cold gas in the circum-galactic medium (CGM); we explore simple analytic models and fitting functions to recent hydrodynamical simulations; (ii) local variations in the ionizing background due to ionizing sources that cluster around the central galaxy. We account for clustering by boosting the observationally inferred volumetric production rate of ionizing photons,  $\epsilon_{\text{LyC}}$ , by a factor  $1 + \xi_{\text{LyC}}(r)$ , in which  $\xi_{\text{LyC}}(r)$  quantifies the clustering of ionizing sources around the central galaxy. We compute  $\xi_{\text{LyC}}(r)$  by assigning an “effective” bias parameter to the ionizing sources. This novel approach allows us to quantify our ignorance of the population of ionizing sources in a simple parametrized form. We find a maximum enhancement in the local ionizing background in the range  $50 - 200$  at  $r \sim 10$  physical kpc. For spatially uncorrelated ionizing sources and fluorescing clouds we find that fluorescence can contribute up to  $\sim 50 - 60\%$  of the observed spatially extended Ly $\alpha$  emission. We briefly discuss how future observations can shed light on the nature of Ly $\alpha$  halos around star forming galaxies.

*Subject headings:* Galaxy: evolution – Galaxy: halo – galaxies: structure – radiative transfer – cosmic background radiation

## 1. INTRODUCTION

The gaseous region out to 300 kpc around galaxies, the so called circum-galactic medium (CGM), plays an important role when it comes to studying the properties and characteristics of the galaxy population (e.g., Bahcall & Spitzer 1969). The CGM connects galaxies and the intergalactic medium (IGM), via gas accretion inflows and feedback-driven outflows. Therefore, studying these regions at different redshifts provides invaluable information about the properties, formation and evolution of galaxies (e.g., Steidel et al. 2010, 2011; Tumlinson et al. 2011; Dijkstra & Kramer 2012; Cantalupo et al. 2012, 2014; Rahmati et al. 2015).

The Lyman alpha (Ly $\alpha$  hereafter) radiation, which corresponds to the transition from the  $2^2\text{P}$  state to the ground state of the hydrogen atom with a line centre wavelength at 1215.67 Å, provides an excellent tool for studying hydrogen gas in the CGM (see Barnes et al. 2014; Dijkstra 2014; Hayes 2015, for detailed reviews). The CGM has been detected in Ly $\alpha$  absorption using galaxy-galaxy (e.g., Rudie et al. 2012), galaxy-quasar (e.g., Rakic et al. 2012) and quasar-quasar (e.g., Hennawi & Prochaska 2013; Prochaska et al. 2013) pairs. However, Ly $\alpha$  has also been observed in emission around low redshift galaxies (e.g., Östlin et al. 2009; Guaita et al. 2015), radio-loud galaxies (RLG; e.g., Saito et al.

2015) and Ly $\alpha$  blobs (e.g., Fynbo et al. 1999; Steidel et al. 2000; Matsuda et al. 2004; Saito et al. 2006; Ao et al. 2015). In addition, recent analyses have indicated that all star forming galaxies may be surrounded by a faint Ly $\alpha$  emission from the CGM, at surface brightness levels of  $\sim 10^{-19} \text{ erg s}^{-1} \text{ cm}^{-2} \text{ arcsec}^{-2}$ . Some studies used stacking analyses to uncover this faint signal out to  $\sim 100$  physical kpc (e.g., Hayashino et al. 2004; Steidel et al. 2011; Matsuda et al. 2012; Momose et al. 2014, 2015), although not all obtained positive detections (Jiang et al. 2013; Feldmeier et al. 2013). Individual detections have also been reported, and some of them account for the inclusion of the spectra (e.g., Wisotzki et al. 2015, see also Rauch et al. (2008a,b)). The Ly $\alpha$  spectral line shape contains information on the gas kinematics (Shapley et al. 2003; Verhamme et al. 2006; Dijkstra & Kramer 2012), while the spatial extent of Ly $\alpha$  emission (and absorption) traces the spatial distribution of hydrogen gas (Steidel et al. 2010, 2011).

The origin of the spatially extended Ly $\alpha$  emission around galaxies (Ly $\alpha$  halos; LAHs) can be attributed to (i) scattering: neutral hydrogen gas in the CGM can scatter Ly $\alpha$  photons that were produced in the inner part of galaxies, and which subsequently escaped from the interstellar medium (see, e.g., Laursen & Sommer-Larsen 2007; Laursen et al. 2011; Zheng et al. 2010; Steidel et al. 2011; Zheng et al. 2011; Dijkstra & Kramer 2012; Verhamme et al. 2012); and (ii) *in situ* production: Ly $\alpha$  can be emitted by hydrogen atoms in the CGM following collisional excitation and/or recombination. Colli-

<sup>1</sup> l.m.ribas@astro.uio.no

sional excitation of the Ly $\alpha$  transition in atomic hydrogen by free electrons reduces the thermal energy - and thus cools - the circum-galactic gas (e.g., Haiman et al. 2000; Fardal et al. 2001; Dijkstra & Loeb 2009; Faucher-Giguère et al. 2010; Rosdahl & Blaizot 2012). Radiative ionizations can produce Ly $\alpha$  photons in a process called ‘fluorescence’: ionizing photons that are produced inside a galaxy (Furlanetto et al. 2005; Weidinger et al. 2005; Nagamine et al. 2010), but also those photons coming from distant sources such as quasars or other galaxies (Haiman & Rees 2001; Alam & Miralda-Escudé 2002; Cantalupo et al. 2005; Adelberger et al. 2006; Cantalupo et al. 2007; Rauch et al. 2008a,b; Kollmeier et al. 2010; Hennawi & Prochaska 2013; Cantalupo et al. 2014), can photoionize the circum-galactic hydrogen which recombines almost immediately. Approximately 66% (42%) of the recombinations<sup>2</sup> produce Ly $\alpha$  for case-B (case-A) recombination (Gould & Weinberg 1996). It is currently still unclear what the main physical mechanism behind LAHs is, and what their relation with the more luminous Ly $\alpha$  ‘blobs’ is.

In this work, we revisit the effect of fluorescence. This is motivated by the observed dependence of Ly $\alpha$  surface brightness profiles on the local overdensity: as the mean number of Ly $\alpha$  emitting galaxies within a sphere of radius  $\sim 2$  Mpc  $h^{-1}$  increases, the spatial extent of the Ly $\alpha$  halos increases (Steidel et al. 2011; Matsuda et al. 2012; Chiang et al. 2015). This dependence is naturally expected when the Ly $\alpha$  emission is powered by fluorescence, as we expect the (average) intensity of the ionizing radiation field to be enhanced in overdense regions. Our main goal is to investigate whether, and under which conditions, fluorescence in the CGM can give rise to the observed Ly $\alpha$  halos (and their dependence on overdensity). This is an interesting question to address because, as we will show in this work, it constrains spatial variations in the ionizing background, which in turn relate to the escape of ionizing photons from galaxies. Our work focuses on Ly $\alpha$  emitters (LAEs) at redshift  $z = 3.1$ . This allows us to compare with the work by Matsuda et al. (2012), who presented their results with respect to LAE overdensity at this redshift. At  $z = 3.1$  stellar radiation provides the major contribution to the ionizing background (e.g., Faucher-Giguère et al. 2008). In a companion paper, we will focus on the contribution of Ly $\alpha$  emission from satellite galaxies to LAHs.

The outline of this paper is as follows: we present our main formalism for computing the surface brightness in fluorescent Ly $\alpha$  in § 2. This formalism shows that the two key model ingredients are (i) the local photoionization rate  $\Gamma(r)$ , and (ii) the distribution of neutral hydrogen gas in the CGM. We present the models for the calculation of these ingredients in § 3, and we show our main results in § 4. We discuss the shortcomings of our model in § 5, before concluding in § 6.

## 2. GENERAL FORMALISM

<sup>2</sup> Note that absorption of higher-order Lyman series photons can also give rise to fluorescent Ly $\alpha$  emission. This process can increase Ly $\alpha$  emission as discussed in, e.g., Furlanetto et al. (2005).

In this section, we introduce the general formalism for the calculation of the Ly $\alpha$  surface brightness profile. This will highlight the main ingredients that have to be assessed in more detail, namely (i) the characteristics of the circum-galactic medium around the central galaxy, and (ii) the ionizing radiation field affecting this medium.

It is well known that the environment of galaxies contains cold optically thick gas (e.g., Bosma 1981; Bergeron 1986; Kunth et al. 1998; Mo & Miralda-Escudé 1996; Steidel et al. 2010). We assume that the central galaxy contains a spherically symmetric distribution of cold gas clumps embedded within a hot medium. It is important to mention here that our formalism does not take into account a correlation between self shielding gas and the surrounding ionizing sources, thus making our calculations conservative. We briefly discuss the importance of this correlation for the boost of the fluorescent signal in § 5. The distribution of clumps can be characterized by their ‘covering factor’,  $f_c(r)$ , which denotes the number of self-shielding clumps along a differential length at a distance  $r$  from the central galaxy (which in the present paper we consider to be an LAE). Many useful quantities can be expressed in terms of  $f_c(r)$ .

For example, the total number of clumps along a sightline at impact parameter  $b$  is  $N_{\text{clump}}(b) = \int_{-\infty}^{\infty} ds f_c(r[b, s])$ , where  $s$  denotes the line-of-sight coordinate. The distance from the galaxy is  $r = \sqrt{b^2 + s^2}$ , and so we can write

$$N_{\text{clump}}(b) = 2 \int_b^{\infty} \frac{r dr}{\sqrt{r^2 - b^2}} f_c(r) . \quad (1)$$

The parameter  $N_{\text{clump}}(b)$  denotes the *average* number of clumps, and the actual number at a given impact parameter fluctuates around this mean due to the discrete nature of the clumps. The probability of finding *at least* one clump at impact parameter  $b$  is  $P(N \geq 1) = 1 - P(N = 0)$ , where  $P(N = 0)$  denotes the Poisson probability of finding no clumps at impact parameter  $b$ . For a Poisson distribution, the probability of finding at least one clump at impact parameter  $b$  is therefore

$$P(N_{\text{clump}} \geq 1, b) = 1 - \exp(-N_{\text{clump}}(b)) . \quad (2)$$

The quantity  $P(N_{\text{clump}} \geq 1, b)$  is useful when comparing to recent results from hydrodynamical simulations.

We can also compute the Ly $\alpha$  surface brightness produced by fluorescence at a given impact parameter  $b$  from  $f_c(r)$  as

$$SB_{\text{Ly}\alpha}(b) = \int_{-\infty}^{\infty} ds P_{\text{clump}}(b, s) SB_{\text{Ly}\alpha}^{\text{clump}}(b, s) , \quad (3)$$

where  $P_{\text{clump}}(b, s)ds = f_c(b, s)ds = f_c(r)ds$  denotes the differential probability of finding a clump along within the range  $s \pm ds/2$ , in which  $s$  denotes the line-of-sight coordinate. Furthermore,  $SB_{\text{Ly}\alpha}^{\text{clump}}(b, s) = SB_{\text{Ly}\alpha}^{\text{clump}}(r) = SB_{\text{Ly}\alpha}^{\text{HM}} \times \frac{\Gamma_{\text{HI}}(r)}{\Gamma_{\text{HI}}^{\text{HM}}}$ . Here  $SB_{\text{Ly}\alpha}^{\text{HM}} = 3.67 \times 10^{-20} [(1+z)/4]^{-4}$  erg s<sup>-1</sup> cm<sup>-2</sup> arcsec<sup>-2</sup>, is the value obtained for fluorescence by Cantalupo et al. (2005) for a photoionization rate  $\Gamma_{\text{HI}}^{\text{HM}} = 1.15 \times 10^{-12}$  s<sup>-1</sup>. Rewriting as above we

obtain

$$SB_{\text{Ly}\alpha}(b) = \frac{2 SB_{\text{Ly}\alpha}^{\text{HM}}}{\Gamma_{\text{HI}}^{\text{HM}}} \int_b^\infty \frac{r dr}{\sqrt{r^2 - b^2}} f_c(r) \Gamma_{\text{HI}}(r), \quad (4)$$

where we emphasize that  $\Gamma_{\text{HI}}(r)$  denotes the photoionization rate at a distance  $r$  from the central galaxy. This ‘local’ photoionization rate can differ significantly from the overall background that is inferred from, e.g., Ly $\alpha$  forest studies.

Eq. 4 highlights two key ingredients that determine the Ly $\alpha$  surface brightness. These include:

1. The covering factor,  $f_c(r)$ , which describes the spatial distribution of self-shielding clouds in the CGM.
2. The value of the local photoionization rate,  $\Gamma_{\text{HI}}(r)$ , which is determined by ionizing sources surrounding the galaxy, as well as the ionizing luminosity from the central galaxy.

It is worth stressing that both these ingredients are difficult to model from first principles: (i) the distribution of cold gas in the CGM depends on the adopted feedback prescriptions (e.g., Faucher-Giguère et al. 2015; Faucher-Giguère et al. 2016). Recent observations indicate that there is a substantial amount of cold gas locked up in small ( $\sim$  tens of pc) dense clumps not resolved in cosmological simulations (e.g., Cantalupo et al. 2014; Hennawi et al. 2015); (ii) The radial dependence of  $\Gamma_{\text{HI}}$  depends on the escape fraction of ionizing photons from both the central galaxy and surrounding galaxies. The escape fraction of ionizing photons, and its dependence on redshift and galaxy type, is still highly uncertain. Given these uncertainties, it is useful to have an analytic formalism which allows for an efficient exploration of the parameter space. We describe both model ingredients in more detail in the following section.

### 3. CHARACTERISING THE CGM AND $\Gamma_{\text{HI}}(r)$

We divide this section into two parts: in the first, we describe our models for  $\Gamma_{\text{HI}}(r)$  [§ 3.1], and in the second, we describe our models for the CGM [§ 3.2].

#### 3.1. Modeling $\Gamma_{\text{HI}}(r)$

We divide the total photoionization rate  $\Gamma_{\text{HI}}(r)$  at a distance  $r$  from the central galaxy into (i) the contribution from the central galaxy itself,  $\Gamma_{\text{HI}}^{\text{cen}}(r)$ , and (ii) the contribution from all other ionizing sources,  $\Gamma_{\text{HI}}^{\text{ext}}(r)$ , i.e.,

$$\Gamma_{\text{HI}}^{\text{tot}}(r) = \Gamma_{\text{HI}}^{\text{cen}}(r) + \Gamma_{\text{HI}}^{\text{ext}}(r). \quad (5)$$

We discuss each component separately below.

##### 3.1.1. Modeling $\Gamma_{\text{HI}}^{\text{cen}}(r)$

The photoionization rate due to the central galaxy at distance  $r$  is

$$\Gamma_{\text{HI}}^{\text{cen}}(r) = f_{\text{esc}}(r) \times \text{SFR} \times \frac{\dot{n}_{\text{ion}} \sigma_{\text{HI}}^{912}}{4\pi r^2} \frac{\gamma}{\gamma - 3}, \quad (6)$$

where  $\dot{n}_{\text{ion}} = 10^{53} \text{ s}^{-1}$  is the total number of ionizing photons emitted per unit SFR and time, where SFR denotes the star formation rate in  $\text{M}_\odot \text{ yr}^{-1}$ .  $\sigma_{\text{HI}}^{912}$  is the hydrogen photoionization cross-section at the Lyman limit frequency,  $\nu_{912}$ , which has a value  $\sigma_{\text{HI}}^{912} = 6.3 \times 10^{-18} \text{ cm}^2$ . We assume that the spectral energy distribution (SED) of a galaxy near the Lyman limit is given by  $L(\nu) = L_{912} (\frac{\nu}{\nu_{912}})^\gamma$ , where we take  $\gamma = -2$  following the work of Becker & Bolton (2013), although the value for this parameter is a matter of debate covering the range between -1 and -3 (see discussions in Kuhlen & Faucher-Giguère 2012; Becker & Bolton 2013). We include the radial dependence of the escape fraction of ionizing photons in terms of  $f_c(r)$  as

$$f_{\text{esc}}(r) = \exp \left[ - \int_0^r f_c(r) dr \right]. \quad (7)$$

For simplicity we assume that  $f_{\text{esc}}(r=0) = 100\%$  and that the radial dependence of  $f_{\text{esc}}$  is determined entirely by the self-shielding clumps. We show in Figure 3 that in our models  $f_{\text{esc}}$  reduces to values that are in good agreement with existing observational constraints. We can account for additional absorption of ionizing photons in the ISM (or molecular clouds) of the galaxy by imposing  $f_{\text{esc}}(r=0) < 100\%$ . This restriction simply scales down our predictions by the same factor.

##### 3.1.2. Modeling $\Gamma_{\text{HI}}^{\text{ext}}(r)$

The photoionization rate due to the external galaxies surrounding the central LAE can be obtained by summing the contribution of all of them as

$$\Gamma_{\text{HI}}^{\text{ext}}(r) = \frac{\sigma_{\text{HI}}^{912} \gamma}{4\pi(\gamma - 3)} \sum_i \frac{\dot{N}_{\text{ion},i}}{|\vec{r} - \vec{r}_i|^2} \exp \left( - \frac{|\vec{r} - \vec{r}_i|}{\lambda_{\text{mfp}}} \right), \quad (8)$$

where the effective ionizing emissivity of galaxy ‘i’ is defined as  $\dot{N}_{\text{ion},i} \equiv \dot{n}_{\text{ion},i} \times \text{SFR}_i \times f_{\text{esc},i}$ ,  $\lambda_{\text{mfp}}$  denotes the effective mean free path of ionizing photons, and where we assumed that each source of ionizing radiation has the same spectral slope  $\gamma$ . The continuous version of Eq. 8 can be written as

$$\begin{aligned} \Gamma_{\text{HI}}^{\text{ext}}(r) &= \frac{\sigma_{\text{HI}}^{912} \gamma}{4\pi(\gamma - 3)} \int dV' \frac{\epsilon_{\text{LyC}}(r')}{|\vec{r} - \vec{r}'|^2} \exp \left( - \frac{|\vec{r} - \vec{r}'|}{\lambda_{\text{mfp}}} \right) \\ &= \frac{\sigma_{\text{HI}}^{912} \gamma}{4\pi(\gamma - 3)} \int_0^\infty r'^2 dr' \int_0^\pi \sin \theta d\theta \\ &\quad \times \int_0^{2\pi} d\phi \frac{\epsilon_{\text{LyC}}(r')}{y(r', \theta, \phi)^2} \exp \left( - \frac{y(r', \theta, \phi)}{\lambda_{\text{mfp}}} \right), \end{aligned} \quad (9)$$

where  $y = \sqrt{r'^2 + r^2 - 2rr' \sin \theta \sin \phi}$ . Here,  $\epsilon_{\text{LyC}}(r')$  denotes the effective production rate of ionizing photons per unit volume. This quantity is poorly constrained as it depends on a number of factors including (i) the non-linear clustering of galaxies around the central galaxy as a function of their  $L_{\text{UV}}$ , and (ii) the escape fraction of

TABLE 1  
PARAMETERS FOR THE CALCULATION OF THE IONIZING  
BACKGROUND.

$z$	$\langle\epsilon_{\text{LyC}}\rangle^{\text{a}}$ [ $10^{50} \text{ s}^{-1} \text{ cMpc}^{-3}$ ]	$f_{\text{esc}}^{\text{b}}$	$\lambda_{\text{mfp}}^{\text{a}}$ [pMpc]
3.1	2.7	0.026	84.4

<sup>a</sup> Values from Table 2 in Kuhlen & Faucher-Giguère (2012).

<sup>b</sup> Average escape fraction of ionizing photons computed using Eq. (14) in Kuhlen & Faucher-Giguère (2012), with the parameters  $\zeta_{\text{ion}} = 1$ ,  $\kappa = 2$  and assuming an  $f_{\text{esc}}(z = 4) = 0.04$ .

ionizing photons as a function of  $L_{\text{UV}}^3$ . We can express  $\epsilon_{\text{LyC}}(r)$  as

$$\epsilon_{\text{LyC}}(r) = \langle\epsilon_{\text{LyC}}\rangle[1 + \xi_{\text{LyC}}(r)], \quad (10)$$

where  $\langle\epsilon_{\text{LyC}}\rangle$  denotes the cosmic average production rate of ionizing photons per unit volume. Importantly,  $\langle\epsilon_{\text{LyC}}\rangle$  can be obtained directly from observations, by combining measurements of  $\lambda_{\text{mfp}}$  and photoionization rates from the Ly $\alpha$  forest (see, e.g., Kuhlen & Faucher-Giguère 2012). The use of  $\langle\epsilon_{\text{LyC}}\rangle$  allows us to circumvent the above-mentioned problems related to the integration limits for the luminosity function and the use of assumptions for the escape fraction of ionizing photons. The quantity  $\xi_{\text{LyC}}(r)$  is the two point correlation function and quantifies how ionizing sources are clustered around the central galaxy, and is clearly important in our analysis. In the next section, we present how we calculate  $\xi_{\text{LyC}}(r)$ , and discuss other model assumptions.

### 3.1.3. Model Assumptions

Our approach is the following:

- For the central LAE we assume a  $\text{SFR} = 10 \text{ M}_{\odot} \text{ yr}^{-1}$ .
- We use for  $\lambda_{\text{mfp}}$  and  $\langle\epsilon_{\text{LyC}}\rangle$ , the values shown in Table 1. These values are taken from the work of Kuhlen & Faucher-Giguère (2012) who compiled them from Faucher-Giguère et al. (2008); Songaila & Cowie (2010); Prochaska et al. (2009); Bolton & Haehnelt (2007).
- For the integral over  $r'$  in Eq. 9, we set the lower limit  $r'_{\text{min}} = 10 \text{ pkpc}$ . We tested the value  $r'_{\text{min}} = 5 \text{ pkpc}$  and we have seen that it does not change our results significantly. The upper limit is set to  $r'_{\text{max}} = 100 \lambda_{\text{mfp}}$ , considering the effect of very distant galaxies. We have explicitly tested that the effect of considering a larger limit does not change the results.

<sup>3</sup> We can write out explicitly an expression for  $\epsilon_{\text{LyC}}(r)$  as

$$\epsilon_{\text{LyC}}(r) = \int_0^{\infty} dL_{\text{UV}} \frac{dn}{dL_{\text{UV}}} [1 + \xi(r, L_{\text{UV}})] \dot{n}_{\text{ion}}(L_{\text{UV}}) f_{\text{esc}}(L_{\text{UV}})$$

where  $\frac{dn}{dL_{\text{UV}}}$  denotes the UV-luminosity function (number density of galaxies in the range  $L_{\text{UV}} \pm dL_{\text{UV}}$ ),  $\dot{n}_{\text{ion}}(L_{\text{UV}})$  denotes the production rate of ionizing photons for a galaxy with  $L_{\text{UV}}$ , and  $f_{\text{esc}}$  denotes the escape fraction of ionizing photons.

- We consider that the real space two-point correlation function for ionizing sources,  $\xi_{\text{LyC}}(r)$ , can be described as

$$\xi_{\text{LyC}}(r) = b_{\text{LyC}} b_{\text{LAE}} [\xi(r)_{1\text{h}} + \xi(r)_{2\text{h}}], \quad (11)$$

where we have used that the cross correlation function of two different tracers, each with its own bias, is given by  $\xi_{\text{ab}}(r) = b_{\text{A}} b_{\text{B}} \xi(r)$ . In our case, the first tracer is an LAE, and we take its scale depending bias,  $b_{\text{LAE}}(r)$ , from fitting the data in the work of Ouchi et al. (2010) (See Appendix B.2 for a description of the procedure). The bias  $b_{\text{LyC}}$  denotes an ‘effective’ bias of LyC emitting sources. Since we currently do not know which galaxies are LyC sources, we leave this quantity as a free parameter, proportional to the bias of LAEs by a constant. Our fiducial calculation assumes  $b_{\text{LyC}}(r) = b_{\text{LAE}}(r)$  but we also discuss the effect of considering other values. Finally, the terms  $\xi_{1\text{h}}(r)$  and  $\xi_{2\text{h}}(r)$  denote the 1-halo and 2-halo terms of the two-point correlation function of dark matter. The 2-halo term accounts for clustering of matter in different dark matter halos, while the 1-halo term accounts for clustering of matter within the same halo. In the Appendix B.1, we detail the calculations for the obtention of these correlation functions.

- Matsuda et al. (2012) showed that the LAE overdensity is correlated with the spatial extent of Ly $\alpha$  halos around LAEs. We compute the overdensity of LAEs,  $\delta_{\text{LAE}}$ , within a sphere of  $R = 2 \text{ Mpc h}^{-1}$  around our central galaxy as

$$\delta_{\text{LAE}} = \frac{n_{\text{LAE}} - \bar{n}_{\text{LAE}}}{\bar{n}_{\text{LAE}}} = \frac{3}{R^3} \int_0^R r^2 dr \xi_{\text{LAE}}(r), \quad (12)$$

where  $n_{\text{LAE}}$  is the number of LAEs in the overdense region and  $\bar{n}_{\text{LAE}}$  is the average value in the field. We obtain a value for the overdensity  $\delta_{\text{LAE}} \sim 1.5$ , which will be important when comparing our results with other works.

- For simplicity, we assume that the escape fraction of Ly $\alpha$  photons is  $f_{\text{esc}}^{\text{Ly}\alpha} = 100\%$ . For the case of fluorescence, Ly $\alpha$  photons escape from a medium with a column density  $N_{\text{HI}} \sim 10^{17} \text{ cm}^{-2}$ . For such low column densities the effects of dust are expected to be small (e.g., Gronke et al. 2015, and references therein). Our results can be scaled directly with  $f_{\text{esc}}^{\text{Ly}\alpha}$  assuming that the escape fraction is not spatially dependent.

## 3.2. Modeling the CGM

Below we describe how we parametrize the CGM. We construct models of the CGM using simplified clumpy outflow models following Steidel et al. (2010) in § 3.2.1, and Dijkstra & Kramer (2012) in § 3.2.2. In § 3.2.3 we take an alternative approach, and adopt a fitting formula for the ‘area’ covering factor of self-shielding gas in the cosmological hydrodynamical EAGLE simulations (Rahmati et al. 2015).

### 3.2.1. Steidel et al. (2010) - Clumpy Outflow Model

We follow Steidel et al. (2010) for this model, where optically thick cold clumps are embedded within an outflowing optically thin hot medium, lying within the radial

range  $r_{\min} = 1$  pkpc and  $r_{\max} = 250$  pkpc. The clumps have a constant mass and are in pressure equilibrium with the hot medium, the pressure of the latter varying with distance as  $p(r) \propto r^{-2}$  (Steidel et al. 2010).

The covering factor,  $f_c(r)$ , is given by (Dijkstra & Kramer 2012)

$$f_c(r) = n_c(r) \sigma_c(r), \quad (13)$$

where  $n_c(r)$  denotes the number density of clumps at  $r$  and  $\sigma_c(r)$  denotes their geometric cross-section. These quantities are given by

$$\begin{aligned} \sigma_c(r) &= \pi R_c(r)^2, \\ n_c(r) &= \frac{C_n}{4\pi r^2 v_c(r)}, \end{aligned} \quad (14)$$

where  $R_c(r)$  denotes the cloud radius. Pressure equilibrium dictates that  $R_c = C_r r^{-2/3}$ . The constant of proportionality  $C_r$  is constrained by the observations, and depends on the number of clumps (see Dijkstra & Kramer 2012, for more details). We adopt the value  $C_r = 0.01$ .  $C_n$  is again a free parameter which we set to  $C_n = 10^{-10} \text{ s}^{-1}$ , in order to obtain agreement with the observations in Steidel et al. (2010). For the outflow velocity profile, we assume that the clumps undergo a radial acceleration of the form  $a_c(r) = A r^{-\alpha_v}$ . Under this assumption, the radial velocity profile is (Steidel et al. 2010)

$$v_c(r) = \left( \frac{2A}{\alpha_v - 1} \right)^{1/2} (r_{\min}^{1-\alpha_v} - r^{1-\alpha_v})^{1/2}, \quad (15)$$

for  $\alpha_v > 1$ . We do not take into account values  $\alpha_v \leq 1$  in this work. Furthermore,  $A$  is a constant that sets the velocity at large radius,  $r \rightarrow \infty$ , through  $v_\infty = \sqrt{2A r_{\min}^{1-\alpha_v} / (\alpha_v - 1)}$ . Following Steidel et al. (2010) we set  $v_\infty = 830 \text{ km s}^{-1}$  and  $\alpha_v = 1.4$ . See Figure 2 in Dijkstra & Kramer (2012) and Figure 3 in the Appendix A for the visualization of these parameters.

We note that this simple model was designed to reproduce CGM absorption line data from composite Lyman Break Galaxy (LBG) spectra. For simplicity, we will use this model for the environment of LAEs. This may artificially enhance the cold gas content of our CGM, and we will return to this when we discuss our results. Also, this model assumes spherical symmetry, which does not represent the true complexity of CGM (e.g., Gauthier & Chen 2012).

### 3.2.2. Dijkstra & Kramer (2012) - Decelerated Outflow

In the model presented by Dijkstra & Kramer (2012) the outflow velocity decreases beyond a certain radius. This modification allowed Dijkstra & Kramer (2012) to simultaneously reproduce absorption and emission around LBGs with a simple scattering model. Their velocity profile was constructed by assuming that the radial clumps undergo an additional radial deceleration due to gravity, which dominates beyond some ‘transition’ ra-

dius. The resulting velocity can be written as

$$v_c(r) = 2\sigma \sqrt{\ln\left(\frac{r_{\min}}{r}\right) + \frac{A}{2\sigma^2(1-\alpha_v)} (r^{1-\alpha_v} - r_{\min}^{1-\alpha_v})}, \quad (16)$$

where  $\sigma$  denotes the velocity dispersion and the other parameters denote the same as in the Steidel et al. model. We adopt for our model parameters the same values as in model IV in Dijkstra & Kramer (2012), to whom we refer the reader for a more detailed discussion about the model. The reduced outflow velocity translates to a larger clump number density (Eq. 14), and thus enhanced covering factor, which in turn affects the radial dependence of  $f_{\text{esc}}(r)$  (Eq. 7).

### 3.2.3. Rahmati et al. (2015) - Fit to EAGLE Simulations

Rahmati et al. (2015) provided a fitting formula for the *area covering fraction* of self-shielding gas around simulated galaxies in the EAGLE simulation. This ‘area covering factor’,  $F_{\text{LLS}}$ , denotes the fraction of the total area  $2\pi b db$  at impact parameter  $b$  that is covered by this gas. We can interpret this fraction  $F_{\text{LLS}}$  as the probability that a sightline at impact  $b$  intersects a self-shielding cloud, or more accurately, at least one self-shielding cloud. In other words, we can set  $F_{\text{LLS}}(b) = P(N_{\text{clump}} \geq 1, b)$  (which is the quantity we introduced in § 2). The fitting formula in Rahmati et al. (2015) is

$$F_{\text{LLS}}(x) = 1 - \frac{1}{1 + \left(\frac{L_z}{x}\right)^\alpha} + C \left[ \frac{1}{1 + \left(\frac{L_z}{x}\right)^3} \right] 10^{\frac{z-4}{3}}, \quad (17)$$

where  $x \equiv r/r_{\text{vir}}$ ,  $z$  denotes redshift and  $L_z = AB^z$ , in which  $A, B, C$  and  $\alpha$  are parameters that depend on the type of absorber that is considered. We use the parameters presented in Table 2 of Rahmati et al. (2015) for the case of Lyman Limit Systems (LLS) and velocity width  $\Delta v = 3000 \text{ km/s}$ . We note that the simulations by Rahmati et al. (2015) only include the global ionizing background by Haardt & Madau (2001), i.e., this fitting formula ignores that the photoionization rate in close proximity to galaxies is elevated. The authors argue, however, that this assumption only affects the fitting formula at the 10% level at distances below the virial radius, and we therefore adopt it as it is.

We now use that  $N_{\text{clump}}(b)$  and  $f_c(r)$  are related to each other via an Abel-transform (see Eq. 1). We can invert this transformation and obtain  $f_c(r)$  from  $N_{\text{clump}}(b)$  as

$$f_c(r) = -\frac{1}{\pi} \int_r^\infty \frac{dN_{\text{clump}}}{dy} \frac{dy}{\sqrt{y^2 - r^2}}, \quad (18)$$

where we obtain  $\langle N_{\text{clump}} \rangle$  from  $F_{\text{LLS}} = P(N_{\text{clump}} \geq 1, b)$  by inverting Eq. 2 to get

$$N_{\text{clump}}(b) = -\ln(1 - F_{\text{LLS}}). \quad (19)$$

We can thus convert the fitting formula from Rahmati et al. (2015) into  $f_c(r)$ , once we specify the virial radius  $r_{\text{vir}}$ . For our model we adopt  $r_{\text{vir}} = 80$  pkpc accounting for the values found for host dark matter halos of  $M_h \sim 10^{12} M_\odot$  (e.g., Cooke et al. 2013), which corresponds to the lowest mass for which the fitting formula

is valid. Finally, the upper integration limit in Eq. 18 is  $r \rightarrow \infty$ . However, in practice we use  $r_{max} = 250$  pkpc, which corresponds to the maximum distance at which cold clumps exist in our model, following Steidel et al. (2010). We have verified that this consideration does not affect our main results. Figure 3 in the Appendix shows the values of the escape fraction and the covering fraction for the case of this method.

#### 4. IONIZATION AND SURFACE BRIGHTNESS PROFILES

We present the results for  $\Gamma(r)$  in § 4.1 and  $SB_{Ly\alpha}$  in § 4.2. We restrict our results to distances larger than 10 pkpc since we consider that below this value, the physics governing the processes within the central galaxy is not accurately represented by our simple methodology.

##### 4.1. Radial Profile $\Gamma_{HI}(r)$

We show in Figure 1 the enhancement of the ionizing background in the medium surrounding the central LAE for our three models. The *thick yellow solid line* shows the contribution from the central galaxy and the *blue dotted line* denotes the contribution from the external galaxies, where we adopted  $b_{LyC}(r) = b_{LAE}(r)$  and considered non-linear clustering. The *green solid line* shows the total photoionization rate, which is simply the sum of the central and external contributions.

Figure 1 shows that photoionization by the central source dominates at small distances for all models. At precisely what radius external galaxies contribute equally depends on the model. Most notably, external galaxies start dominating closer to the central galaxy (at  $r \sim 30$  pkpc) in the Rahmati et al. model because the photoionization rate from the central galaxy lies significantly lower than in the other two models. This is because in this model  $f_c(r)$  is larger at small  $r$ , which causes  $f_{esc}$  to have dropped to a lower value at  $r = 10$  pkpc compared with the other two models.

In any case, in all models the enhancement of the photoionization rate is substantial: a factor  $\gtrsim 10$  at  $r \lesssim 30$  kpc, and goes up to a factor of  $\sim 50$  ( $\gtrsim 250$ ) at  $r \sim 10$  pkpc for the Rahmati et al. model (Steidel et al. and Dijkstra & Kramer models). At larger  $r$ , we recover the average value for the ionizing background, although we find the value  $\Gamma_{HI} \sim 4 \times 10^{-13} \text{ s}^{-1}$ , which is slightly smaller than the result obtained by Kuhlen & Faucher-Giguère (2012),  $\Gamma_{HI} \sim 6 \times 10^{-13} \text{ s}^{-1}$ . This difference arises from the value for the spectral slope, which we adopted from Becker & Bolton (2013) for our calculations (see § 3.1.1), but it does not affect our results significantly.

##### 4.2. Radial Profile Surface Brightness $SB_{Ly\alpha}(b)$

Figure 2 shows the  $Ly\alpha$  surface brightness profiles for our three models, as given by Eq. 4. For comparison, we show a simplified view of the data for the highest density range,  $2.5 < \delta_{LAE} < 5.5$ , in Matsuda et al. (2012) (their upper-left panel in Figure 3).

The *left panel* shows the Steidel et al. model, which predicts a surface brightness that lies a factor  $\sim 1.5$  below the observations at  $10 < r < 30$  pkpc. This factor varies slightly at larger distances but the general behaviour is well reproduced. For this model, the central galaxy dominates the profile up to  $r \sim 70$  pkpc and the contribution from external galaxies is only important at larger distances. However, the strong impact of the central galaxy requires a very high ionizing photon escape fraction at distances below 50 pkpc ( $\sim 30\%$ ; Figure 3). The *middle panel* of Figure 2 shows the Dijkstra & Kramer model. The high covering factor,  $f_c$ , at large distances yields a profile which is significantly above the observed data (a factor  $\sim 3$  at  $r \sim 65$  pkpc). The *right panel* denotes the Rahmati et al. model which presents a profile significantly below the observed data, a factor  $\sim 3$  ( $\sim 8$ ) at  $r \sim 10$  ( $r \sim 65$ ) pkpc. This is because in this model  $f_c$  and  $f_{esc}$  are much smaller at large  $r$  (see Figure 3), which reduces the surface brightness. We note that the Steidel et al. and Dijkstra & Kramer models were designed to reproduce observations of (the more massive) LBGs, and may therefore overpredict the surface brightness.

Rahmati et al. (2015) formally adopted an ionizing background that was  $\sim 3$  times higher than ours when calculating  $F_{LLS}(b)$ , which affects their covering fraction at large distances. We note however, that the small differences that this introduces in the predicted fluorescent surface brightness are sub-dominant to differences introduced by local enhancements in the ionizing background.

We remind here that our overdensity value is  $\delta_{LAE} \sim 1.5$  and we are comparing to the range  $2.5 < \delta_{LAE} < 5.5$  in Matsuda et al. (2012). In § C in the Appendix we show the results obtained when simply changing the value for the LAE bias (setting it to twice its default value) to obtain an overdensity  $\delta_{LAE} \sim 5.8$ . Also, we show the case when setting  $b_{LyC}(r) = 3 b_{LAE}(r)$  to test the effects of a different bias for the ionizing sources. However, as we show, these variations do not affect our main results.

#### 5. DISCUSSION OF THE MODEL

There are several effects that we did not include in our modeling. First, our analysis assumes that the self-shielding clumps and ionizing sources are spatially uncorrelated. This assumption is likely unrealistic: for realistic cosmological density fields there are azimuthal density fluctuations at fixed galacto-centric radius  $r$ , and we expect both ionizing sources and self-shielding gas to preferentially reside in higher density regions<sup>4</sup>. If ionizing sources and self-shielding gas are spatially correlated, then this boosts the fluorescent signal: suppose that the local ionizing flux that is “seen” by a self-shielding cloud is due to a single nearby source, and that the spatial correlation between ionizing sources and self-shielding gas reduces the separation  $d$  between the nearest ionizing source and the self-shielding gas by a factor of  $x$  (i.e.  $d \rightarrow xd$ , where  $x < 1$ ), then this boosts the local ionizing flux by a factor of  $x^{-2}$ . This can be a big effect. We note

<sup>4</sup> An example of such an azimuthal density fluctuation occurs when both the self-shielding gas and the ionizing sources reside in filaments that connect to the central galaxy

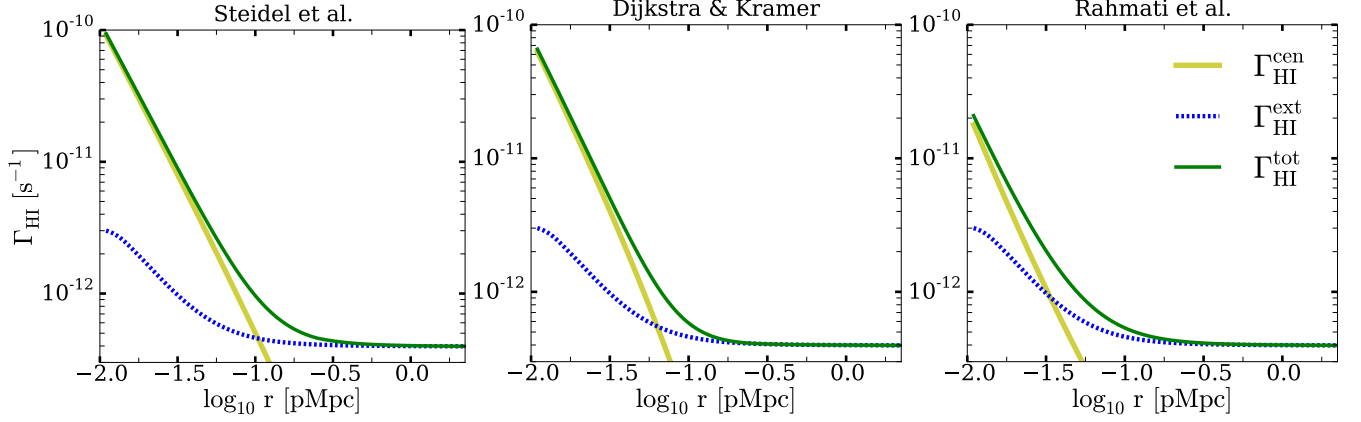


FIG. 1.— Enhancement of the ionizing radiation with radial distance around the central LAE, expressed in terms of the photo-ionization rate, using  $b_{\text{LyC}}(r) = b_{\text{LAE}}(r)$  for our three models. The *thick yellow line* indicates the contribution of the central LAE. The *dashed blue line* denotes the effect produced by the external galaxies and the *continuous green line* shows the addition of the two. Note the small contribution of the external galaxies to the boost, except for the case of the Rahmati et al. model. At a distance  $r \sim 10$  pkpc, the boost in the ionizing background reaches a factor of  $\sim 50$  for the Rahmati et al. case and  $\gtrsim 200$  for the other two models.

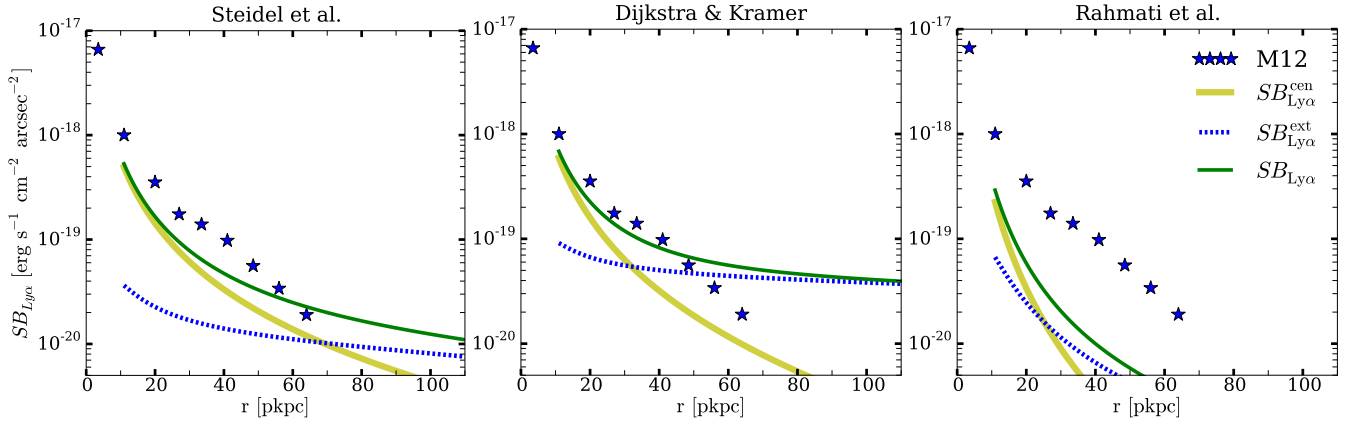


FIG. 2.—  $\text{Ly}\alpha$  surface brightness profiles for our three CGM models assuming  $b_{\text{LyC}}(r) = b_{\text{LAE}}(r)$  and  $f_{\text{esc}}^{\text{Ly}\alpha} = 100\%$ . The x-axis denotes the impact parameter in physical units. The *thick yellow line* shows the profile due to the central LAE and the *blue dashed line* the contribution from the external galaxies. The *continuous green line* shows the total surface brightness profile and the stars denote a simple estimation of the data in Matsuda et al. (2012), for their overdensity range  $2.5 < \delta_{\text{LAE}} < 5.5$ . The Steidel et al. and Dijkstra & Kramer models, where the effect of the central galaxy is very important, are close to the observed data. The latter, however, shows a signal at large distances, due to the effect of the external galaxies, above the observations. The Rahmati et al. model is well below the data and only the central galaxy approaches the observations at very small distances.

however, that by introducing a spatial correlation between the self-shielding gas and ionizing sources, we force the observed  $\text{Ly}\alpha$  emission to closely trace the sources of ionizing radiation, which likely causes this model to predict that the non-ionizing UV continuum surface brightness profile should closely trace that of  $\text{Ly}\alpha$ . This is in disagreement with the observations in overdense regions by Steidel et al. (2010); Matsuda et al. (2012) although Momose et al. (2015) argues that a possible UV signal from the external galaxies may be within the current detection threshold.

Second, we assumed that  $\text{Ly}\alpha$  photons are observed from the location where they were produced. In reality we may expect  $\text{Ly}\alpha$  photons to also scatter off the self-shielding gas clouds. Scattering redistributes the emission in the halo, and serves to flatten the predicted surface brightness profile (e.g., Zheng et al. 2011; Hansen & Peng Oh 2006; Dijkstra & Kramer 2012; Laursen &

Sommer-Larsen 2007).

Third, we have (purposefully) ignored other in-situ  $\text{Ly}\alpha$  production mechanisms. Clustering of ionizing sources surrounding the central galaxy may also give rise to clustering of  $\text{Ly}\alpha$  emitting sources around the central galaxy, as the sources of ionizing radiation are also sources of  $\text{Ly}\alpha$  photons. We will address the contribution of satellite galaxies to the extended  $\text{Ly}\alpha$  emission in a follow up paper. Our main formalism can be easily modified to quantify this contribution.

Fourth, we have ignored the contribution of possible cooling radiation ( $\text{Ly}\alpha$  emission produced via collisional excitation in the neutral gas in response to, e.g., gravitational heating). We note that LAEs are thought to reside in low mass halos ( $M_h \sim 10^{11.5} M_\odot$ , e.g., Gawiser et al. 2007). Predicted  $\text{Ly}\alpha$  cooling luminosities is a difficult problem which carries several uncertainties (e.g., Dijkstra & Loeb 2009; Faucher-Giguère et al. 2010; Can-

talupo et al. 2012). Predictions for  $M_h \sim 10^{11.5} M_\odot$  are that  $L_{Ly\alpha} \sim 10^{42} \text{ erg s}^{-1}$  (Dijkstra & Loeb 2009; Faucher-Giguère et al. 2010; Goerdt et al. 2010; Rosdahl & Blaizot 2012), and can reach a surface brightness  $\gtrsim 10^{-19} \text{ erg s}^{-1} \text{ cm}^{-2} \text{ arcsec}^{-2}$  at  $r \approx 20 \text{ pkpc}$  (see Fig 13 of Rosdahl & Blaizot 2012).

Lake et al. (2015) reproduced the  $Ly\alpha$  surface brightness profile around LAEs naturally in their cosmological hydrodynamical simulations through a combination of cooling and satellite galaxies. Given the above mentioned uncertainties related to CGM modeling, it would be interesting to explore the constraints that this places on various subgrid prescriptions in the simulations. We will investigate the contribution from satellites to the  $Ly\alpha$  surface brightness in a parameterized way in the companion paper. This will complement the work by Lake et al. (2015).

## 6. SUMMARY AND CONCLUSIONS

Fluorescence refers to the conversion of ionizing photons into  $Ly\alpha$  on the surface of self-shielding gas in the circum-galactic medium (see § 1). We have computed whether fluorescence can explain spatially extended  $Ly\alpha$  halos which have been ubiquitously observed around star forming galaxies.

We have presented a general formalism for calculating the signal from fluorescence in § 2. This formalism shows that there are two key model ingredients: (i) the distribution of self-shielding gas in the circum-galactic medium, which is quantified via its (differential) covering factor,  $f_c(r)$ , which denotes the number of self-shielding clumps per unit length; (ii) the local ionizing radiation field, which is quantified by the photoionization rate  $\Gamma(r)$ . Here,  $r$  denotes the galacto-centric distance from the galaxy. We argued in § 2 that it is not possible yet to model/simulate these quantities from first principles. It is therefore useful to have an analytic formalism which allows for an efficient exploration of the parameter space.

We presented our model for  $\Gamma(r)$  in § 3.1, which accounts for the distance dependent escape fraction of ionizing flux from the central galaxy. We also consider clustering of ionizing sources around the central galaxy, by boosting the *observationally inferred* volumetric production rate of ionizing photons,  $\epsilon_{LyC}$ , by a factor  $1 + \xi_{LyC}(r)$ , in which  $\xi_{LyC}(r)$  quantifies the clustering of ionizing sources around the central galaxy. The nature of ionizing sources is still unknown, and we assumed that  $\xi_{LyC}(r) = b_{LyC} b_{LAE} \xi(r)$ , in which  $\xi(r)$  denotes the non-linear matter two-point correlation function,  $b_{LAE}$  is the scale dependent bias for LAEs from Ouchi et al. (2010) and  $b_{LyC}$  is an ‘effective’ bias parameter for the ionizing sources. Our fiducial model assumed (for simplicity) that  $b_{LyC} = b_{LAE}$ . We stress that *this approach allowed us to quantify our ignorance of the population of ionizing sources simply with a single parameter inferred from studies of the  $Ly\alpha$  forest*,  $\epsilon_{LyC}$ , and  $b_{LyC}$ .

To model  $f_c(r)$ , we have taken three different ap-

proaches (see § 3.2). In the *first*, we follow Steidel et al. (2010) who presented a simple analytic model for  $f_c(r)$  which was tuned to reproduce the observed  $Ly\alpha$  absorption from the CGM (obtained from galaxy-galaxy pairs, see § 3.2.1). In the *second*, we include the modification by Dijkstra & Kramer (2012) in the form of a decelerated outflow. For the *third*, we adopt a fitting formula provided by Rahmati et al. (2015) for the *area covering fraction* of self-shielding gas around simulated galaxies in the EAGLE simulation, which we convert into  $f_c(r)$  via an inverse Abel-transform (see § 3.2.3).

Our results can be summarized as follows:

- We find that the ‘local’ ionizing background is boosted by a factor  $\sim 50$  ( $\sim 200$ ) at  $r = 10 \text{ pkpc}$ , where external clustered sources of ionizing radiation dominate at  $r \gtrsim$  a few tens ( $r \gtrsim 80 - 100$ )  $\text{pkpc}$  for the analytical model (two clumpy outflow models). These differences arise from the different ionizing photon escape fraction profiles. Smaller values for  $f_{esc}$  reduce the contribution of the central galaxy to the local ionizing radiation field.
- Our predicted surface brightness profile for the accelerated clumpy outflow model falls a factor of  $\sim 1.5 - 2$  below the observations at  $r \lesssim 30 \text{ pkpc}$  and maintains this reasonable fit at larger distances. This implies that fluorescence may account for 50-60% of the observed flux. The model with the decelerated outflow shows a profile above the observations at distances  $r \gtrsim 50 \text{ pkpc}$ . The model for the fit to the EAGLE simulations predicts a surface brightness which is a factor 3-8 below the observations depending on distance (even considering a highly clustered population of ionizing sources,  $b_{LyC} = 3b_{LAE}$ ).
- If fluorescence is to reproduce the observed surface brightness profiles, then this requires that (i) a significant fraction of cold gas, i.e., high covering factor,  $f_c$ , must be present at large distances from the center of the galaxy. (ii) A significant escape fraction of ionizing photons from the central galaxy at small distances is required for the central galaxy to reproduce the observations at such distances, and (iii) the  $Ly\alpha$  escape fraction has to be close to 100%. Otherwise, fluorescence only accounts for a fraction of the flux in  $Ly\alpha$  halos.

There are significant uncertainties associated with predicting the fluorescent  $Ly\alpha$  flux in halos surrounding star forming galaxies, including the unknown nature of sources of ionizing radiation and the gaseous content of the CGM. These uncertainties represent key uncertainties in our understanding of galaxy formation and evolution, and in how ionizing (and  $Ly\alpha$ ) photons escape from the interstellar media of galaxies. Our calculations indicate that a contribution from fluorescence to the total flux in the halo is possible, and more if ionizing sources and self-shielded gas are correlated. This correlation may help to reduce the contribution to the fluorescent  $Ly\alpha$  surface brightness from the central galaxy at  $r \sim 30-70 \text{ pkpc}$ . If the central galaxy was entirely responsible for the fluorescent signal at these impact parameters, then this may make it difficult to the environmental dependence of the scale-length of LAHs (and the



non-dependence on  $M_{UV}$  of the central galaxy, Steidel et al. 2011; Matsuda et al. 2012; Momose et al. 2015; Wisotzki et al. 2015).

In spite of theoretical uncertainties, we expect rapid progress in this field due to anticipated improvements in the quality of incoming data. As our previous discussion illustrates, comparing the Ly $\alpha$  and UV continuum surface brightness profiles provides useful constraints on the models. Another very useful observable is the spectrum. With integral field spectrographs such as MUSE<sup>5</sup> it is possible to constrain the spatially resolved spectrum. As alluded to in § 1, the Ly $\alpha$  spectral line shape contains information on the kinematics of the scattering medium. Different models for Ly $\alpha$  halos generally predict different Ly $\alpha$  spectra, and how they vary with position. Spectra of Ly $\alpha$  created as fluorescence have been predicted to be narrow, and double peaked (e.g., Gould & Weinberg 1996; Cantalupo et al. 2005). Further into the future, it would be extremely valuable to use, e.g., JWST<sup>6</sup> and/or future ground-based facilities such as E-ELT<sup>7</sup> or GMT<sup>8</sup> to search for spatially extended H $\alpha$  emission. H $\alpha$  emission is also produced by fluorescence, but does not resonantly scatter through neutral hydrogen gas. Future joint H $\alpha$  and Ly $\alpha$  observations of halos would provide independent constraints on all these halos. Independently, measurements of the polarization of Ly-alpha would differentiate between models that invoke scattering and in-situ production to explain the observed spatially extended Ly-alpha halos (see, e.g., Dijkstra & Loeb 2008; Dijkstra & Kramer 2012). First detections of polar-

ization in spatially extended Ly $\alpha$  emission have recently been reported (Hayes et al. 2011; Humphrey et al. 2013; Beck et al. 2016, and also see Prescott et al. (2011) for a non-detection), which provide independent constraints on the models.

While none of these measurements are easy, and their interpretation complicated, it is important to understand Ly $\alpha$  halos, as they contain information on the gaseous content of the CGM which complements that of absorption line studies (e.g., Dijkstra & Kramer 2012; Hennawi & Prochaska 2013), and on the amplitude of the local ionizing radiation field. The latter contains information on quantities like the escape fraction, and on the nature of ionizing sources in general. Both of these questions represent some of the main uncertainties in our understanding of the reionization process, and the physical properties of the galaxies in general.

We are grateful to the anonymous referee, whose constructive comments allowed for a significant improvement of our work. We thank Alireza Rahmati for comments about the Rahmati et al. model. We acknowledge Stuart Wyithe and Avi Loeb for their opinions and ideas. We thank Max Gronke for useful discussions about the clumpy medium and the importance of the escape fraction around and within galaxies; we also thank Brendan Griffen, Maxime Trebitsch and J.Xavier Prochaska for their advice in clustering aspects. We thank the astronomy department at Columbia University and at UC Santa Barbara for their kind hospitality.

## APPENDIX

### PARAMETERS OF THE CLUMPY CIRCUM-GALACTIC MEDIUM

*Blue solid lines* in Figure 3 show the parameters of the clumpy outflow model using the method of Steidel et al. (2010). The decelerated outflow model by Dijkstra & Kramer (2012) (their model IV) is represented by the *dot-dashed green lines* where the two models present differences. *Dashed red lines* denote the parameters computed from the results by Rahmati et al. (2015). From left to right and top to bottom, we present the outflow velocity  $v_c(r)$ , the radius of the clumps  $R_c(r)$ , the area of the clumps  $\sigma_c(r)$ , the number density of clumps  $n_c(r)$ , the covering factor  $f_c(r)$  and the escape fraction of ionizing photons  $f_{esc}(r)$ . All these values are shown with respect to the distance from the central LAE. We can see that the covering factor for the case of the Rahmati et al. model presents a much steeper decay at large distances compared to the other two models, although it reaches higher values at small distances. This enhances the number of clumps close to the centre and reduces it at large distances, which in turn, makes the escape fraction to suffer a very strong decrease within a few tens of kpc. At the maximum distance of our calculations,  $r = 250$  pkpc, the three methods reach an escape fraction value consistent with other works; The Steidel et al. model yields a value around 15%, Rahmati et al. around 5% and Dijkstra & Kramer model around 0%. As a reference, the work by Kuhlen & Faucher-Giguère (2012) finds a value for the average escape fraction  $\sim 3\%$  at  $z = 3$  (Table 1). This value is inferred from studies of the Ly $\alpha$  forest although large differences are obtained between works concerning galaxy surveys.

### NON-LINEAR CLUSTERING OF LAES

Clustering of LAEs is commonly addressed making use of a power law of the form

$$\xi(r) = \left( \frac{r}{r_0} \right)^{\alpha_c}, \quad (\text{B1})$$

<sup>5</sup> <http://www.eso.org/sci/facilities/develop/instruments/muse.html>

<sup>6</sup> <http://jwst.nasa.gov/index.html>

<sup>7</sup> <https://www.eso.org/sci/facilities/eelt/>

<sup>8</sup> <http://www.gmto.org/>

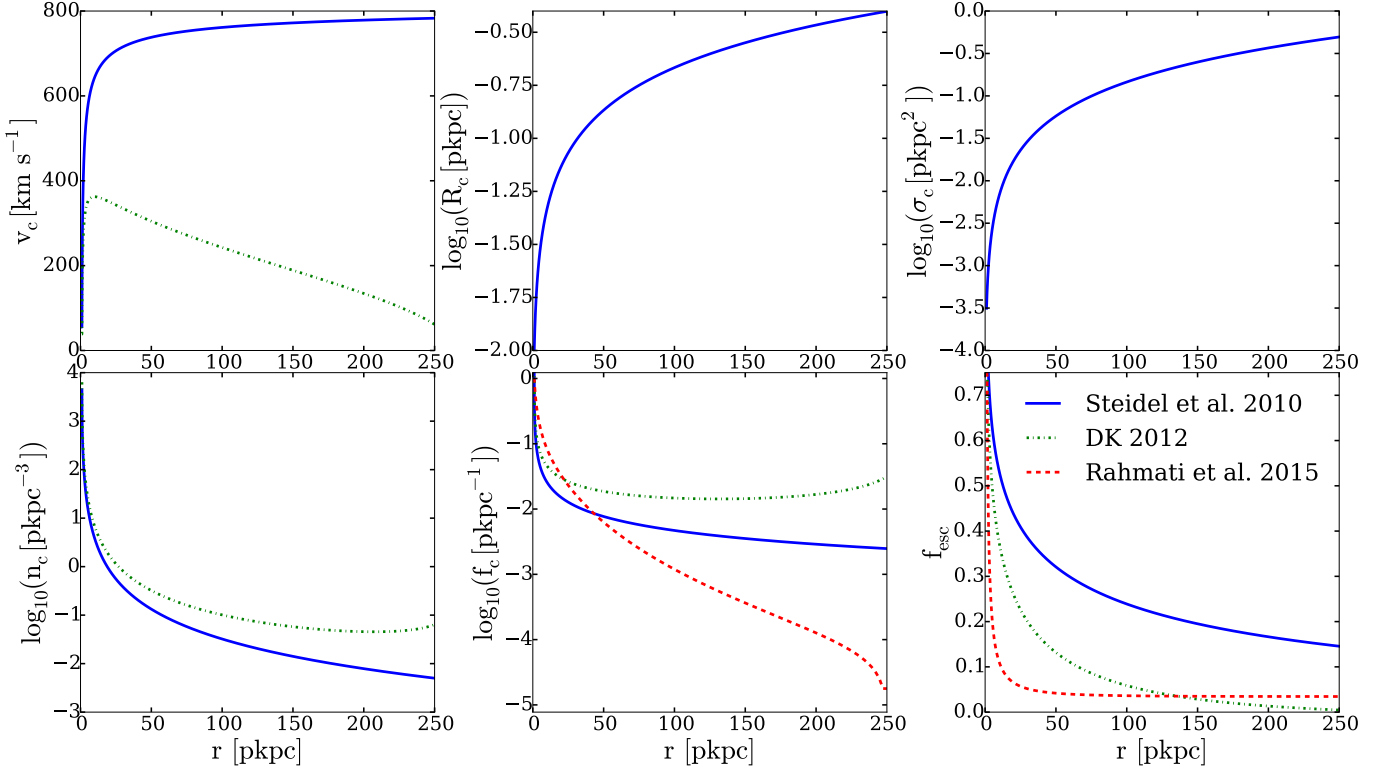


FIG. 3.— Parameters for the clumpy outflow model with respect to distance from the central LAE. *Blue solid line* denotes the Steidel et al. method and the *green dot-dashed line* that of Dijkstra & Kramer. The covering factor and escape fraction computed from the results by Rahmati et al. are also shown as *dashed red line*. Note the large differences for the case of the covering factor and escape fraction using the Rahmati et al. formalism compared to the other two outflowing models. See the text above for the description of the parameters.

with values  $r_0 \sim 2.5 \text{ Mpc h}^{-1}$  (this parameter depending on redshift) and  $\alpha_c \sim -1.8$  (e.g., Bielby et al. 2015; Gawiser et al. 2007; Kovač et al. 2007; Ouchi et al. 2003, 2010; Guaita et al. 2010). However, for the purpose of our work, we are interested in the effect due to galaxies at small distances from the central LAE. This cannot be taken into account using a power law but a proper non-linear clustering treatment is necessary (Iliev et al. 2003; Sheth et al. 2001b). In order to address this more realistic clustering analysis, we make use of the *halo model* (see, e.g., Zheng & Guo 2015; Sheth et al. 2001a,b; Smith et al. 2003; Peacock & Dodds 1996, and also Cooray & Sheth (2002) for an extensive description), which has been largely used in order to reproduce simulations and observations providing satisfactory results (e.g., Genel et al. 2014; Tal et al. 2013; Sales et al. 2007; Nagai & Kravtsov 2005). We construct an initial matter power spectrum<sup>9</sup> (see, e.g., Peacock & Dodds 1994, for a review on the calculation of the linear matter power spectrum) and use the publicly available software *hmf*<sup>10</sup> to compute the non-linear matter power spectrum at the redshift of interest. Once we have the power spectrum, we compute the non-linear matter two-point correlation function as  $\xi(r) = \xi(r)_{1h} + \xi(r)_{2h}$ . Finally, we make a simple fit to the data of Ouchi et al. (2010) to obtain the scale dependent bias of LAEs. Below, we describe this two step procedure in more detail.

### Non-linear matter power spectrum and correlation function

We compute the non-linear matter power spectrum using *hmf*, adopting the default settings except for the redshift at which the calculation is performed. *hmf* makes use of the software CAMB (Lewis et al. 2000) to compute the transfer function, and applies the non-linear corrections to the power spectrum using the HALOFIT (Smith et al. 2003) model, with the updated parameters from Takahashi et al. (2012) (see a detailed description of the method in <https://github.com/steven-murray/hmf>). For these calculations, a  $\Lambda$ CDM cosmological model with parameters  $\Omega_\Lambda = 0.6825$ ,  $\Omega_b = 0.049$ ,  $h = H_0/100 = 0.67$  and  $\sigma_8 = 0.8344$  is assumed. Left panel in Figure 4 shows the computed matter power spectrum, where the effect of the non-linear clustering can be observed as a change in the slope between  $k \sim 1 \text{ Mpc}^{-1} h$  and  $k \sim 10 \text{ Mpc}^{-1} h$ , thus enhancing the power at small scales, i.e., large  $k$ . Once the power spectrum is computed, the correlation function can be easily obtained using the Fourier transform of the former as

$$\xi_{DM}(r) = \frac{1}{4\pi^2} \int dk k^2 P(k) \frac{\sin(kr)}{kr}, \quad (\text{B2})$$

<sup>9</sup> We consider that the dark matter power spectrum is the same as the matter power spectrum, since the former is the major contributor to the latter.

<sup>10</sup> <https://github.com/steven-murray/hmf>

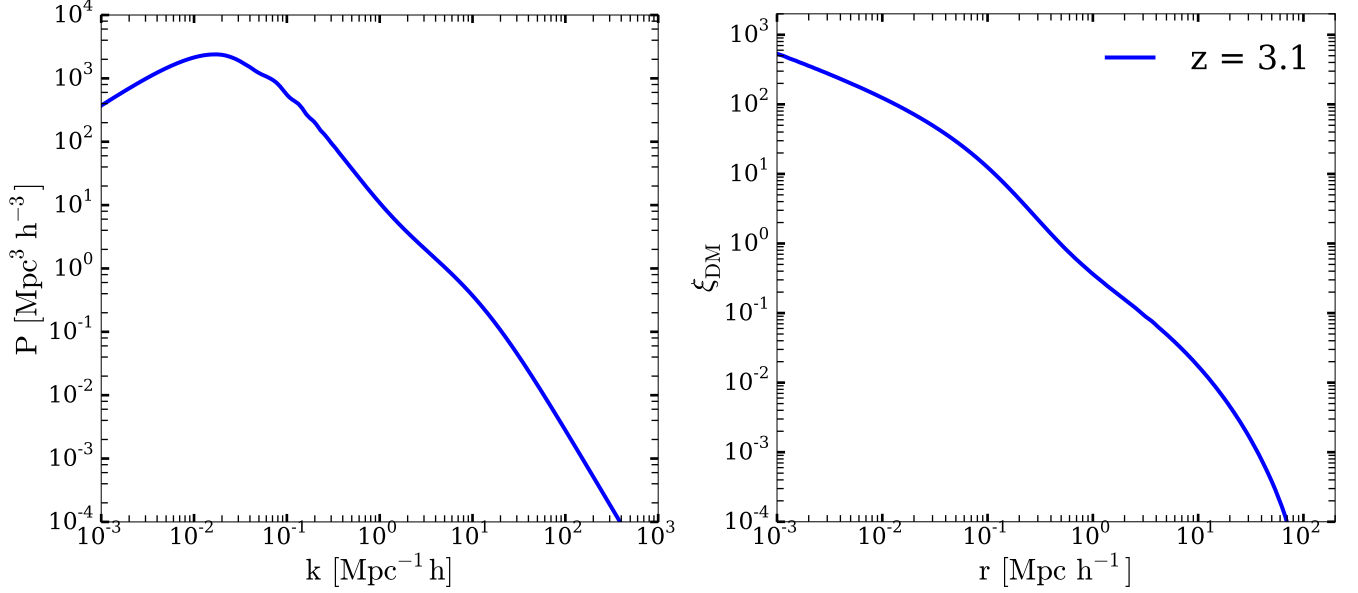


FIG. 4.— *Left panel:* The matter power spectrum computed at redshift  $z = 3.1$ . Notice the effect of the non-linear clustering between  $k \sim 1 \text{ Mpc}^{-1} \text{h}$  and  $k \sim 10 \text{ Mpc}^{-1} \text{h}$  seen as a change in the slope which produces an enhancement of the power at small scales. *Right panel:* The two-point correlation function for dark matter. The 2-halo term dominates at distances larger than  $r \sim 1 \text{ Mpc h}^{-1}$  and denotes the linear clustering term in the correlation. The 1-halo term, denoting the clustering of sources inside the same dark matter halo, dominates at shorter scales and is the responsible for the enhanced non-linear part of the correlation function.

where  $k$  is the wavenumber. The right panel in Figure 4 shows the correlation function for dark matter. The contribution of the two halo terms is clearly visible: at distances larger than  $r \sim 1 \text{ Mpc h}^{-1}$  the 2-halo term dominates, denoting the linear part of the correlation. At shorter distances, the 1-halo term is the responsible for the non-linear effect that raises the value of the correlation function at those scales.

#### Bias and LAE correlation function

The final step for the calculation of the correlation function of LAEs is to consider the bias between LAEs and dark matter, which is described as

$$b_{\text{LAE}}^2(r) = \frac{\xi_{\text{LAE}}(r)}{\xi_{\text{DM}}(r)}. \quad (\text{B3})$$

We use the data in Ouchi et al. (2010) who provides the scale dependent bias for LAEs at several redshifts. The presence of faint sources below the observability threshold or the resolution power makes the observation of clustering very difficult (Gawiser et al. 2007; Kovač et al. 2007; Ouchi et al. 2010). Due to this, we find only three data points at distances  $r < 0.4 \text{ Mpc h}^{-1}$  (see lower left panel in Figure 11 in Ouchi et al. 2010). We perform a linear fit to the data points, in log-log representation, and assume the constant average bias computed by Ouchi et al. (2010),  $b_{\text{LAE}} \sim 1.5$ , for larger distances. We note that the resulting correlation function of LAEs at small scales is very sensitive to the value of the distance dependence bias. However, an unavailable larger number of data points would be required to obtain a more reliable fit at such distances. The left panel in Figure 5 shows the bias profile and the data from Ouchi et al. (2010) and the right panel the resulting LAE correlation function.

#### EFFECTS OF VARYING THE GALAXY BIAS

We show here the surface brightness profiles obtained when allowing small variations of the galaxy bias. We address two cases: (i) We consider the effect of a higher LAE overdensity since in our work we have been comparing to the highest density case from Matsuda et al. (2012). We do this simply by doubling the default value of  $b_{\text{LAE}}$ . We call this bias  $b_{\text{LAE}}^{2x}$  and its total effect is an increase a factor 4 for the correlation function. We adopt this simple procedure because we ignore how the clustering profile of a ‘more’ overdense region may change compared to the computed one. The overdensity value is now  $\delta_{\text{LAE}} \sim 5.8$ , slightly above the maximum value of Matsuda et al. (2012). (ii) We also consider a departure from the LAE bias when considering the bias of ionizing sources. We assess the value  $b_{\text{LyC}}(r) = 3 \times b_{\text{LAE}}(r)$ . Larger values appear to be not physically motivated to us. In this case, the total effect is a boost a factor 3 for the correlation function, so we expect to find very similar results in the two cases.

Figure 6 shows the results for these two calculations. Due to the similar total effect to the correlation function, there are no significant differences between the two methods. More important, there are no significant changes when

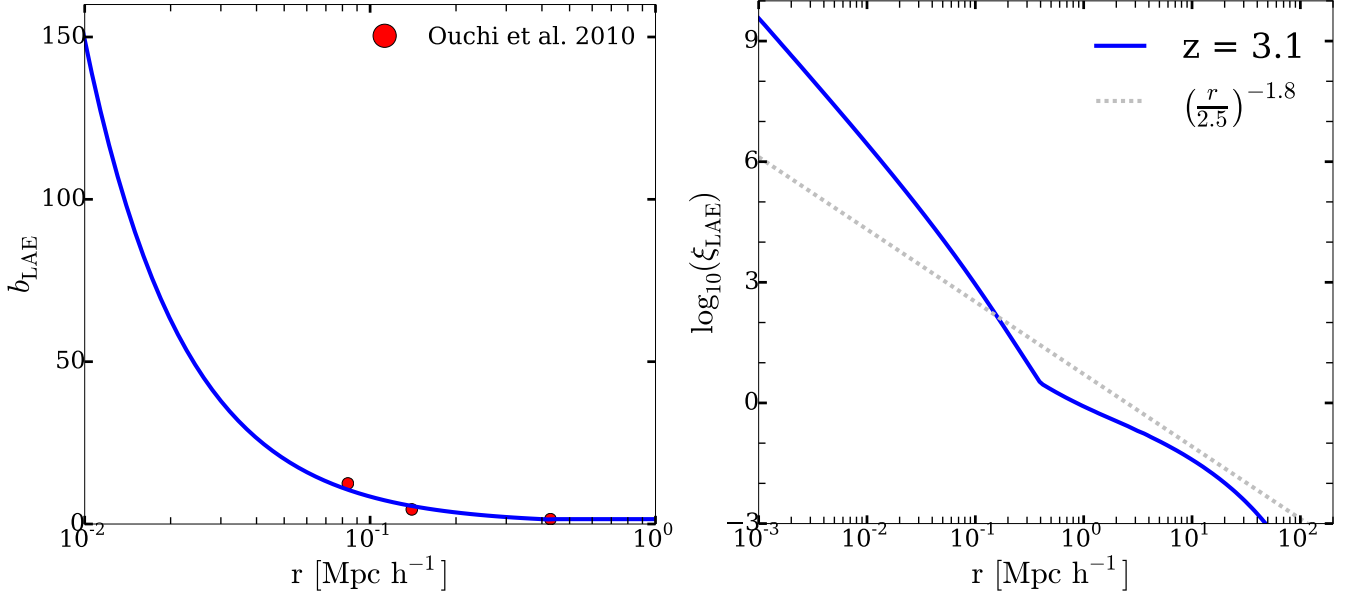


FIG. 5.— *Left panel:* The distance dependent bias for the case of LAEs. The *red dots* denote the data points from Ouchi et al. (2010) used for fitting the bias profile. *Right panel:* The *blue solid line* denotes the correlation function for LAEs. For comparison, the *grey dashed line* represents a commonly adopted correlation function with correlation length  $r_0 = 2.5 \text{ Mpc h}^{-1}$  and power law index  $\alpha = -1.8$ .

comparing to our default model parameters. Thus, our main conclusions are not very sensitive to small variations of the bias parameter but they are strongly dependent on the properties of the medium.

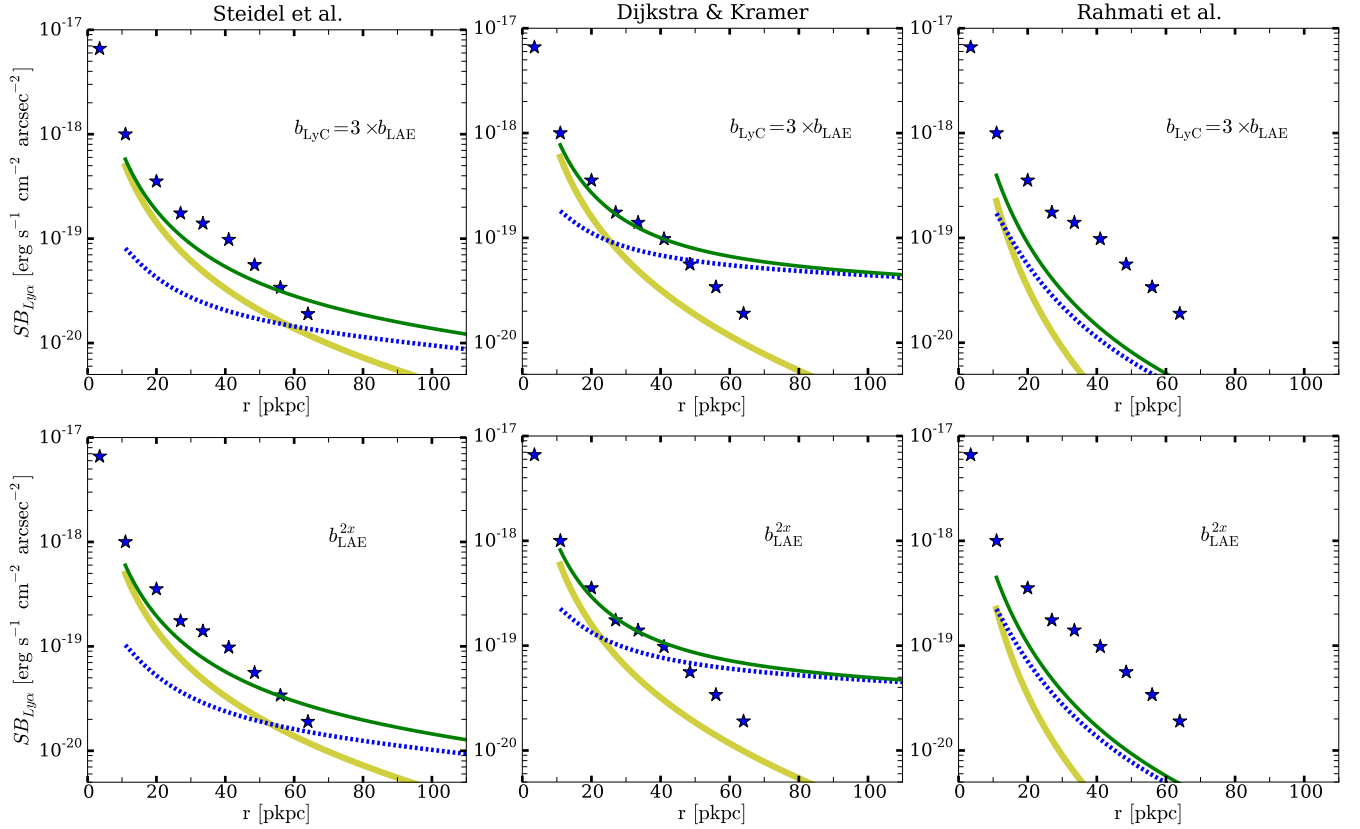


FIG. 6.— *Upper panels* show the surface brightness profile when accounting for a different bias between LAEs and ionizing sources. *Lower panels* show the profiles when doubling the LAE bias in order to recover higher overdensities. The markers and lines are the same as in Figure 2. Due to the similar total effect, there are very small differences between the two cases. There are also small differences with our default models which do not change our main results.

## REFERENCES

- Adelberger, K. L., Steidel, C. C., Kollmeier, J. A., & Reddy, N. A. 2006, *ApJ*, 637, 74
- Alam, S. M. K., & Miralda-Escudé, J. 2002, *ApJ*, 568, 576
- Ao, Y., Matsuda, Y., Beelen, A., et al. 2015, *A&A*, 581, A132
- Bahcall, J. N., & Spitzer, Jr., L. 1969, *ApJL*, 156, L63
- Barnes, L. A., Garel, T., & Kacprzak, G. G. 2014, *PASP*, 126, 969
- Beck, M., Scarlata, C., Hayes, M., Dijkstra, M., & Jones, T. J. 2016, *ArXiv e-prints*, arXiv:1601.06786
- Becker, G. D., & Bolton, J. S. 2013, *MNRAS*, 436, 1023
- Bergeron, J. 1986, in *Astrophysics and Space Science Library*, Vol. 121, *Structure and Evolution of Active Galactic Nuclei*, ed. G. Giuricin, M. Mezzetti, M. Ramella, & F. Mardirossian, 421–434
- Bielby, R. M., Tummuangpak, P., Shanks, T., et al. 2015, *ArXiv e-prints*, arXiv:1501.01215
- Bolton, J. S., & Haehnelt, M. G. 2007, *MNRAS*, 382, 325
- Bosma, A. 1981, *AJ*, 86, 1791
- Cantalupo, S., Arrigoni-Battaia, F., Prochaska, J. X., Hennawi, J. F., & Madau, P. 2014, *Nature*, 506, 63
- Cantalupo, S., Lilly, S. J., & Haehnelt, M. G. 2012, *MNRAS*, 425, 1992
- Cantalupo, S., Lilly, S. J., & Porciani, C. 2007, *ApJ*, 657, 135
- Cantalupo, S., Porciani, C., Lilly, S. J., & Miniati, F. 2005, *ApJ*, 628, 61
- Chiang, Y.-K., Overzier, R. A., Gebhardt, K., et al. 2015, *ApJ*, 808, 37
- Cooke, J., Omori, Y., & Ryan-Weber, E. V. 2013, *MNRAS*, 433, 2122
- Cooray, A., & Sheth, R. 2002, *Phys. Rep.*, 372, 1
- Dijkstra, M. 2014, *PASA*, 31, 40
- Dijkstra, M., & Kramer, R. 2012, *MNRAS*, 424, 1672
- Dijkstra, M., & Loeb, A. 2008, *MNRAS*, 386, 492
- , 2009, *MNRAS*, 400, 1109
- Fardal, M. A., Katz, N., Gardner, J. P., et al. 2001, *ApJ*, 562, 605
- Faucher-Giguère, C.-A., Feldmann, R., Quataert, E., et al. 2016, *ArXiv e-prints*, arXiv:1601.07188
- Faucher-Giguère, C.-A., Hopkins, P. F., Kereš, D., et al. 2015, *MNRAS*, 449, 987
- Faucher-Giguère, C.-A., Kereš, D., Dijkstra, M., Hernquist, L., & Zaldarriaga, M. 2010, *ApJ*, 725, 633
- Faucher-Giguère, C.-A., Lidz, A., Hernquist, L., & Zaldarriaga, M. 2008, *ApJ*, 688, 85
- Feldmeier, J. J., Hagen, A., Ciardullo, R., et al. 2013, *ApJ*, 776, 75
- Furlanetto, S. R., Schaye, J., Springel, V., & Hernquist, L. 2005, *ApJ*, 622, 7
- Fynbo, J. U., Møller, P., & Warren, S. J. 1999, *MNRAS*, 305, 849
- Gauthier, J.-R., & Chen, H.-W. 2012, *MNRAS*, 424, 1952
- Gawiser, E., Francke, H., Lai, K., et al. 2007, *ApJ*, 671, 278
- Genel, S., Vogelsberger, M., Springel, V., et al. 2014, *MNRAS*, 445, 175
- Goerdt, T., Dekel, A., Sternberg, A., et al. 2010, *MNRAS*, 407, 613
- Gould, A., & Weinberg, D. H. 1996, *ApJ*, 468, 462
- Gronke, M., Bull, P., & Dijkstra, M. 2015, *ApJ*, 812, 123
- Guaita, L., Gawiser, E., Padilla, N., et al. 2010, *ApJ*, 714, 255
- Guaita, L., Melinder, J., Hayes, M., et al. 2015, *A&A*, 576, A51
- Haardt, F., & Madau, P. 2001, in *Clusters of Galaxies and the High Redshift Universe Observed in X-rays*, ed. D. M. Neumann & J. T. V. Tran
- Haiman, Z., & Rees, M. J. 2001, *ApJ*, 556, 87
- Haiman, Z., Spaans, M., & Quataert, E. 2000, *ApJL*, 537, L5
- Hansen, M., & Peng Oh, S. 2006, *NAR*, 50, 58
- Hayashino, T., Matsuda, Y., Tamura, H., et al. 2004, *AJ*, 128, 2073
- Hayes, M. 2015, *PASA*, 32, 27
- Hayes, M., Scarlata, C., & Siana, B. 2011, *Nature*, 476, 304
- Hennawi, J. F., & Prochaska, J. X. 2013, *ApJ*, 766, 58
- Hennawi, J. F., Prochaska, J. X., Cantalupo, S., & Arrigoni-Battaia, F. 2015, *Science*, 348, 779
- Humphrey, A., Vernet, J., Villar-Martín, M., et al. 2013, *ApJL*, 768, L3
- Iliev, I. T., Scannapieco, E., Martel, H., & Shapiro, P. R. 2003, *MNRAS*, 341, 81
- Jiang, L., Egami, E., Fan, X., et al. 2013, *ApJ*, 773, 153
- Kollmeier, J. A., Zheng, Z., Davé, R., et al. 2010, *ApJ*, 708, 1048
- Kovač, K., Somerville, R. S., Rhoads, J. E., Malhotra, S., & Wang, J. 2007, *ApJ*, 668, 15
- Kuhlen, M., & Faucher-Giguère, C.-A. 2012, *MNRAS*, 423, 862
- Kunth, D., Mas-Hesse, J. M., Terlevich, E., et al. 1998, *A&A*, 334, 11
- Lake, E., Zheng, Z., Cen, R., et al. 2015, *ArXiv e-prints*, arXiv:1502.01349
- Laursen, P., & Sommer-Larsen, J. 2007, *ApJL*, 657, L69
- Laursen, P., Sommer-Larsen, J., & Razoumov, A. O. 2011, *ApJ*, 728, 52
- Lewis, A., Challinor, A., & Lasenby, A. 2000, *Astrophys. J.*, 538, 473
- Matsuda, Y., Yamada, T., Hayashino, T., et al. 2004, *AJ*, 128, 569
- , 2012, *MNRAS*, 425, 878
- Mo, H. J., & Miralda-Escudé, J. 1996, *ApJ*, 469, 589
- Momose, R., Ouchi, M., Nakajima, K., et al. 2014, *MNRAS*, 442, 110
- , 2015, *ArXiv e-prints*, arXiv:1509.09001
- Nagai, D., & Kravtsov, A. V. 2005, *ApJ*, 618, 557
- Nagamine, K., Choi, J.-H., & Yajima, H. 2010, *ApJL*, 725, L219
- Östlin, G., Hayes, M., Kunth, D., et al. 2009, *AJ*, 138, 923
- Ouchi, M., Shimasaku, K., Furusawa, H., et al. 2003, *ApJ*, 582, 60
- , 2010, *ApJ*, 723, 869
- Peacock, J. A., & Dodds, S. J. 1994, *MNRAS*, 267, 1020
- , 1996, *MNRAS*, 280, L19
- Prescott, M. K. M., Smith, P. S., Schmidt, G. D., & Dey, A. 2011, *ApJL*, 730, L25
- Prochaska, J. X., Worseck, G., & O’Meara, J. M. 2009, *ApJL*, 705, L113
- Prochaska, J. X., Hennawi, J. F., Lee, K.-G., et al. 2013, *ApJ*, 776, 136
- Rahmati, A., Schaye, J., Bower, R. G., et al. 2015, *ArXiv e-prints*, arXiv:1503.05553
- Rakic, O., Schaye, J., Steidel, C. C., & Rudie, G. C. 2012, *ApJ*, 751, 94
- Rauch, M., Haehnelt, M., Bunker, A., et al. 2008a, *ApJ*, 681, 856
- Rauch, M., Haehnelt, M., Bunker, A., et al. 2008b, in *Astronomical Society of the Pacific Conference Series*, Vol. 399, *Panoramic Views of Galaxy Formation and Evolution*, ed. T. Kodama, T. Yamada, & K. Aoki, 59
- Rosdahl, J., & Blaizot, J. 2012, *MNRAS*, 423, 344
- Rudie, G. C., Steidel, C. C., Trainor, R. F., et al. 2012, *ApJ*, 750, 67
- Saito, T., Shimasaku, K., Okamura, S., et al. 2006, *ApJ*, 648, 54
- Saito, T., Matsuda, Y., Lacey, C. G., et al. 2015, *MNRAS*, 447, 3069
- Sales, L. V., Navarro, J. F., Abadi, M. G., & Steinmetz, M. 2007, *MNRAS*, 379, 1475
- Shapley, A. E., Steidel, C. C., Pettini, M., & Adelberger, K. L. 2003, *ApJ*, 588, 65
- Sheth, R. K., Diaferio, A., Hui, L., & Scoccimarro, R. 2001a, *MNRAS*, 326, 463
- Sheth, R. K., Hui, L., Diaferio, A., & Scoccimarro, R. 2001b, *MNRAS*, 325, 1288
- Smith, R. E., Peacock, J. A., Jenkins, A., et al. 2003, *MNRAS*, 341, 1311
- Songaila, A., & Cowie, L. L. 2010, *ApJ*, 721, 1448
- Steidel, C. C., Adelberger, K. L., Shapley, A. E., et al. 2000, *ApJ*, 532, 170
- Steidel, C. C., Bogosavljević, M., Shapley, A. E., et al. 2011, *ApJ*, 736, 160
- Steidel, C. C., Erb, D. K., Shapley, A. E., et al. 2010, *ApJ*, 717, 289
- Takahashi, R., Sato, M., Nishimichi, T., Taruya, A., & Oguri, M. 2012, *ApJ*, 761, 152
- Tal, T., van Dokkum, P. G., Franx, M., et al. 2013, *ApJ*, 769, 31
- Tumlinson, J., Thom, C., Werk, J. K., et al. 2011, *Science*, 334, 948
- Verhamme, A., Dubois, Y., Blaizot, J., et al. 2012, *A&A*, 546, A111
- Verhamme, A., Schaerer, D., & Maselli, A. 2006, *A&A*, 460, 397
- Weidinger, M., Møller, P., Fynbo, J. P. U., & Thomsen, B. 2005, *A&A*, 436, 825

Wisotzki, L., Bacon, R., Blaizot, J., et al. 2015, ArXiv e-prints, arXiv:1509.05143  
Zheng, Z., Cen, R., Trac, H., & Miralda-Escudé, J. 2010, ApJ, 716, 574

Zheng, Z., Cen, R., Weinberg, D., Trac, H., & Miralda-Escudé, J. 2011, ApJ, 739, 62  
Zheng, Z., & Guo, H. 2015, ArXiv e-prints, arXiv:1506.07523